Geophysical Research Letters

RESEARCH LETTER
10.1029/2022GL097834

Key Points:

- Combining ocean observations allows estimation of western boundary current (WBC) variability between 0 m and 1975 m depth over 2004–2019
- A decrease was observed in Kuroshio transport, no significant change was observed in Agulhas or East Australian Current transport
- Transport in all three WBCs is greatest in summer and related to coincident changes in core speed

Supporting Information:

Supporting Information may be found in the online version of this article.

Correspondence to:

M. Chandler,
mlchandler@ucsd.edu

Citation:

Chandler, M., Zilberman, N. V., & Sprintall, J. (2022). Seasonal to decadal western boundary current variability from sustained ocean observations. *Geophysical Research Letters*, *49*, e2022GL097834. https://doi.org/10.1029/2022GL097834

Received 14 JAN 2022
Accepted 10 JUN 2022

Seasonal to Decadal Western Boundary Current Variability From Sustained Ocean Observations

M. Chandler[1], N. V. Zilberman[1], and J. Sprintall[1]

[1]Scripps Institution of Oceanography, University of California San Diego, La Jolla, CA, USA

Abstract Subtropical western boundary currents (WBCs) exert a substantial influence on regional climate. To improve WBC observations on seasonal-to-decadal timescales, and characterize their subsurface structure to 1975 m depth, we combine high-resolution expendable bathythermograph, Argo, and satellite altimetry observations in the Agulhas Current, East Australian Current, and Kuroshio. The resulting 16 year time series (2004–2019) show a weakening trend in Kuroshio transport, but no trend in Agulhas transport or East Australian Current transport. All three WBCs have stronger transport in summer, driven mostly by changes in current speed rather than current width. This unique subsurface view of WBC variability reveals changes in the path of the Kuroshio Extension on interannual timescales, and eddy variability in the Agulhas. Our work highlights how this application of a consistent methodology to combine complementary ocean observations allows for an unprecedented direct comparison of variability between WBCs.

Plain Language Summary Western boundary currents are major ocean currents located on the western side of the world's oceans. These currents transport warm water toward the poles, which influences regional weather and climate. However, despite their importance, the fast speeds, high variability, and narrow width of these currents makes them difficult to observe. Here we examine the western boundary currents (WBCs) of the Indian Ocean (Agulhas Current) and Pacific Ocean (East Australian Current and Kuroshio) using measurements from three different ocean observing networks. The same method is applied to each current, allowing us to compare variability in the three currents. Between the start of 2004 and end of 2019 we find that transport of water has decreased in the Kuroshio but has not changed in the Agulhas or East Australian Current. We find changes in the path of the Kuroshio on interannual time scales, and shorter and irregular changes in the path of the Agulhas. On annual time periods, all three currents transport more water in summer than winter, which is related to faster speeds during the summer. These long subsurface time series can help us better understand how WBC variability impacts society at the western boundaries of the ocean.

1. Introduction

The subtropical western boundary currents (WBCs) are strong, poleward-flowing currents located on the western side of the major ocean basins (Figure 1). They redistribute oceanic mass and heat from low-to mid-latitudes and are vital in the release of heat and moisture to the atmosphere (Cronin et al., 2010; Hu et al., 2015), which influences weather patterns and regional climate (Minobe et al., 2008; Nakamura et al., 2008; Njouodo et al., 2018; Qiu et al., 2014; Sugimoto et al., 2021). Furthermore, changes in these currents impact extreme climate variability. Intensification or changes in the path of WBCs can produce advection-driven marine heatwaves (Oliver et al., 2017, 2021), likewise, variability in WBC strength and proximity to the coast are correlated with local sea-level variability (Archer et al., 2017; Diabaté et al., 2021; Ezer et al., 2013; Holbrook et al., 2011; Nhantumbo et al., 2020; Sasaki et al., 2014).

WBCs are expected to change under a warming climate (Oliver & Holbrook, 2014; Sen Gupta et al., 2021; Yang et al., 2016). Most recently, Sen Gupta et al. (2021) project decreased Kuroshio, Gulf Stream, and Agulhas Current transport, and increased transport in the Brazil Current and extension regions of the East Australian Current (EAC) and Agulhas. However, challenges associated with measuring these currents across multiple time and space scales can cause large uncertainties, even in present-day conditions. Producing long-term transport estimates of these narrow, fast, and highly variable WBCs from a single observing platform is often not feasible. Mooring arrays provide the highest resolution measurements over the full vertical extent of WBCs, but are typically restricted to only a few years and do not always capture the full width of WBCs (e.g., Beal et al., 2015; Bryden et al., 2005; Lee et al., 2001; Mata et al., 2000; Sloyan et al., 2016). On the other hand, broadscale

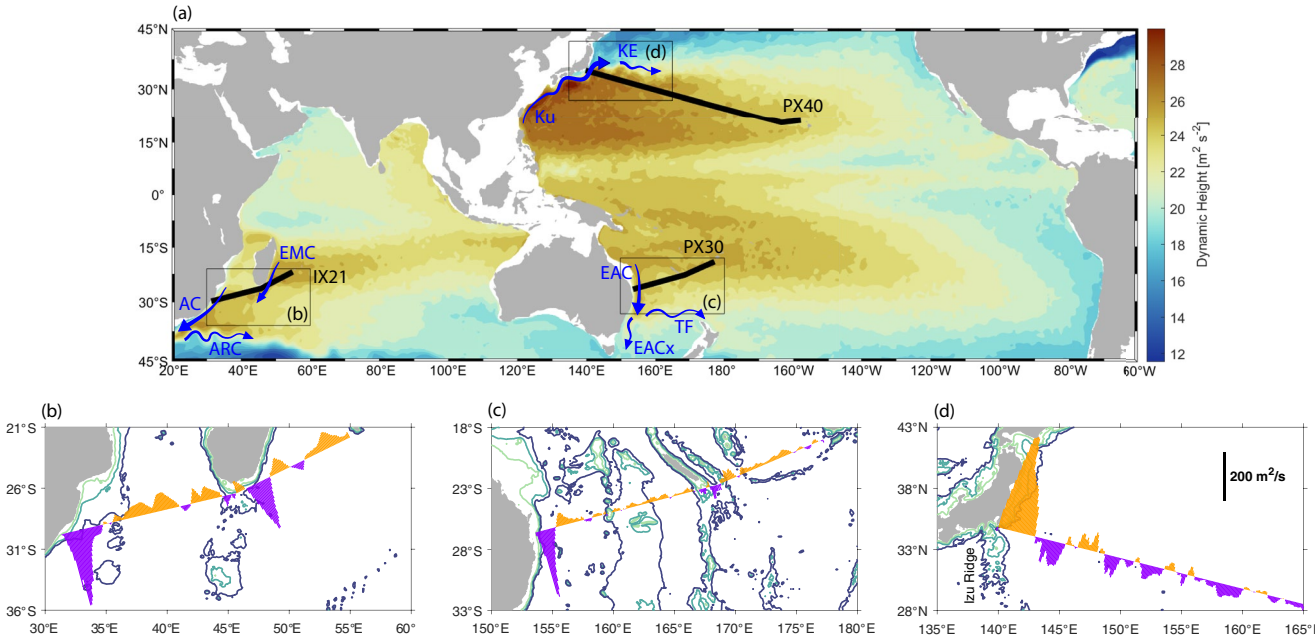

Figure 1. (a) 2004–2018 mean dynamic height at the surface relative to 1975-dbar from Argo (Roemmich & Gilson, 2009), high-resolution expendable bathythermograph (HR-XBT) nominal transects (black), and associated western boundary currents (blue). Abbreviations are: AC - Agulhas Current; ARC - Agulhas Return Current; EMC - East Madagascar Current; EAC - East Australian Current; EACx - East Australian Current Extension; TF - Tasman Front; Ku - Kuroshio; KE - Kuroshio Extension. (b–d) 2004–2019 mean depth-integrated (0–1975 m) absolute geostrophic velocity across mean HR-XBT transects (b) IX21, (c) PX30, and (d) PX40. Depth contours are 200 m (green), 1000 m (blue-green), and 2000 m (blue). Izu Ridge (referred to in the text) is labeled in (d).

observing systems used in the ocean interior - such as Argo - do not adequately sample these narrow and swift WBCs (Riser et al., 2016; Send et al., 2010). Developing WBC time series therefore often requires combining complementary observing platforms (e.g., Beal & Elipot, 2016; Goes et al., 2020; Lee et al., 2001; Liu et al., 2021; Ridgway et al., 2008; Zilberman et al., 2018).

In this study, we examine and compare seasonal-to-decadal variability in the WBCs of the Pacific Ocean (Kuroshio and EAC) and Indian Ocean (Agulhas Current) (Figure 1). Complementary High-Resolution eXpendable BathyThermograph (HR-XBT), Argo, and satellite altimetry observations are combined over their shared 2004–2019 period to produce cross-transect geostrophic velocity estimates down to 1975 m depth at 1 month and 0.1° longitude resolutions (Section 2). These estimates allow us to characterize the subsurface velocity structure over a longer time period than afforded by most other subsurface observations of WBCs. In addition, because a consistent methodology is used, variability is directly comparable between the WBCs. We examine the transport mean, trend, and annual cycle for each WBC, along with variability in the location of each WBC (Section 3).

2. Data and Methods

2.1. Data

HR-XBT transects are occupied nominally 4 times a year and measure temperature to roughly 860 m depth with horizontal resolution of 6–10 km in WBC regions and 25–50 km in the ocean interior (Goni et al., 2019). The Agulhas Current is sampled by IX21 between Durban, South Africa and Port Louis, Mauritius; the EAC by PX30 between Brisbane, Australia and Suva, Fiji; and the Kuroshio by PX40 between Yokohama, Japan and Honolulu, Hawai'i (Figure 1). For each transect, temperature was objectively mapped onto 10 m depth intervals from 0 m to 800 m and 0.1° intervals in longitude (Roemmich, 1983; Zilberman et al., 2018). Corresponding salinity data was obtained using temperature-salinity relationships based on Argo data (Zilberman et al., 2018) and mapped at the same 0.1° resolution as the objectively mapped temperature. Argo profiles to 1975 m depth were used for temperature and salinity (TS) profiles, and Argo trajectory velocities (Scanderbeg et al., 2019) were used to provide reference velocities at 1000 m depth. We also used the 2004–2018 mean Argo TS 1/6° × 1/6° gridded climatologies (Roemmich & Gilson, 2009). The satellite altimetry product used was the daily-mean sea-level

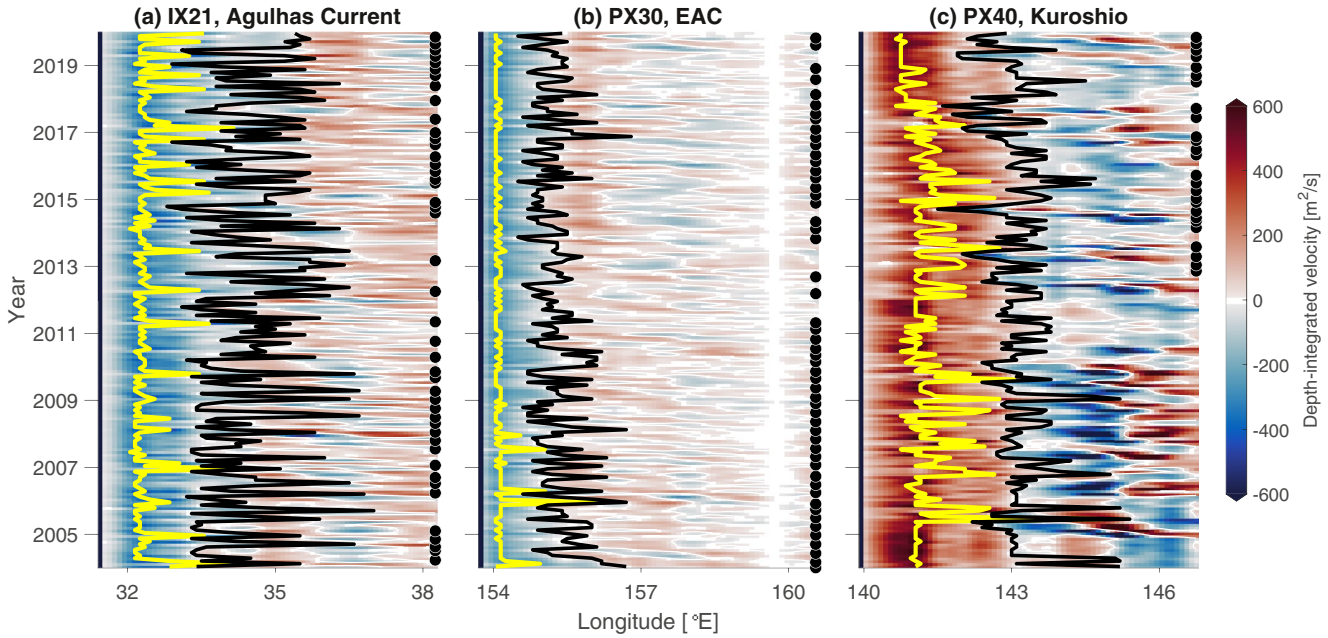

Figure 2. Longitude-time Hovmöller plots of depth-integrated (0–1975 m) absolute geostrophic velocity for the western section of high-resolution expendable bathythermograph (HR-XBT) transects (a) IX21, (b) PX30, and (c) PX40 sampling the Agulhas Current, East Australian Current (EAC), and Kuroshio respectively. Negative values (blue) indicate southward flow. Yellow and black lines identify the core and offshore edge of the western boundary current. Filled circles on the right indicate the dates of HR-XBT transects. Low depth-integrated velocities near 160°E (PX30) are due to a shallow seamount (Figure 1c).

anomaly (SLA) 1/4° × 1/4° gridded product (Taburet et al., 2019). All data sets were for 2004–2019, covering the period since global Argo coverage was first achieved.

2.2. Computing Velocity Estimates

The method used to compute the velocity estimates was based on Zilberman et al. (2018), which the reader is referred to for complete details. Nominal transects (Figure 1) were determined as the linearized average of the 2004–2019 HR-XBT transects. The difference between Argo TS climatologies along individual HR-XBT transects and along the nominal transect were added to HR-XBT TS to produce corrected TS along the nominal transect. Corrected transects were extended from the reference depth (z_{ref}) to 1975 m depth using the linear regression (Ridgway & Godfrey, 1997; Zilberman et al., 2018):

$$h(z/1975) - h(z/z_{ref}) \approx m(z_{ref}) \cdot T_{z_{ref}} + c(z_{ref}), \qquad 0 \le z \le z_{ref} \tag{1}$$

$$h(z/1975) \approx m(z) \cdot T_{z_{ref}} + c(z), \qquad z_{ref} < z \tag{2}$$

where m and c are the regression coefficients, determined using Argo profiles within ±1.5° latitude of the nominal transect that extend to at least 1975 m depth; $T_{z_{ref}}$ is the temperature at z_{ref}; and $h(z/z_1)$ is the steric height (h) at depth z relative to depth z_1. For each transect, z_{ref} (800 m for IX21 and PX30, 600 m for PX40) was selected based on where maximum correlations occurred between h and $T_{z_{ref}}$ from Argo profiles (profile-averaged $r > 0.8$ for all three transects). Steric height was then adjusted to be relative to 1975 m or the bottom depth if shallower (z_b) using bathymetry from Smith and Sandwell (1997).

To obtain monthly estimates of h, daily-mean SLAs were interpolated onto the nominal transect and the time-mean and trend over the HR-XBT measurement period (2004–2019 for IX21 and PX30, 2012–2019 for PX40; Figure 2) were removed to obtain the SLA temporal anomaly (SLA′). Daily-mean SLA′ was averaged over 7 days centered on the HR-XBT WBC sampling date. The h time-mean and trend at each coordinate (x) and depth

were removed to obtain the h temporal anomaly (h'). A linear regression was calculated between h' and the 7 day average SLA′ (Zilberman et al., 2018):

$$h'(z/z_b)(x) \approx m(x,z) \cdot \mathrm{SLA}'(x) + c(x,z) \tag{3}$$

to obtain the regression coefficients m and c. Using these regression coefficients, Equation 3 was applied to monthly-averaged SLA′ to obtain monthly estimates of h', which then had the h trend added back in over the HR-XBT measurement period and h time-mean added back in over 2004–2019. For PX40, where the HR-XBT record is shorter (Figure 2c), our transport estimates compared favorably with observations from the Kuroshio Extension System Study (Donohue et al., 2008, 2010) over June 2004 – October 2005 (Figure S1 in Supporting Information S1) when PX40 was not occupied. This favorable comparison provides confidence in our methodology.

Cross-transect geostrophic velocity (v_g) was calculated from the thermal wind relation (e.g., Gill, 1982) relative to a level of no motion at z_b. Argo trajectory velocities (Scanderbeg et al., 2019) at the nominal parking depth of 1000 ± 100-dbar were used to obtain estimates of cross-transect absolute geostrophic velocity (v) by referencing v_g to this level of known motion:

$$v(z,x,t) = v_g(z,x,t) - \overline{v_g(1000,x)} + \overline{v_\perp(x)} \tag{4}$$

where t is time, the overbar represents the 2004–2019 time-average, and $v_\perp$ is the component of the Argo trajectory velocity perpendicular to the nominal transect. Velocities were referenced to the bathymetry in regions shallower than 1000 m. Mean Argo trajectory velocities were computed using 1/2° longitude × 3° latitude bins centered on the nominal transect (Zilberman et al., 2018). Because WBCs tend to follow the bathymetry near the coast, bins were aligned parallel to the 1000 m isobath in WBC regions. Offshore of the WBCs, in the ocean interior, bins were meridionally oriented. The relatively sparse (Figure S2 in Supporting Information S1) and noisy Argo trajectory velocity data dominates the uncertainty, hence it was not possible to employ a time-varying $v_\perp$ and v uncertainties were assigned based on the standard error of $v_\perp$. Our transport estimates for transects PX40 (Figure S1 in Supporting Information S1) and PX30 (Figure S3 in Supporting Information S1) were validated against independent measurements.

2.3. Metrics of WBC Variability

Four metrics were used to compare WBCs: core longitude, core depth-integrated velocity, offshore edge deviations, and WBC transport (Figure 2). To compute these metrics, v was depth-integrated (0–1975 m) then smoothed along-transect using a triangle filter with size chosen based on the deformation radius in each region (LaCasce & Groeskamp, 2020). The WBC core was defined as where poleward depth-integrated velocities were maximum. The offshore edge was defined as where depth-integrated velocities changed from poleward to equatorward moving offshore from the WBC core. Offshore edge deviations were used, rather than WBC width, as nominal transects are not necessarily perpendicular to the WBC flow (Figure 1). The inshore edge was defined as the western edge of the transect. WBC transport (Figure S4 in Supporting Information S1) was the depth-integrated velocity horizontally integrated between the inshore and offshore edges. The uncertainty on the time-mean WBC transport was assessed using the $v_\perp$ standard error out to the mean offshore edge. To compute annual cycles, time series were smoothed using a 3 month boxcar filter (Figure S4 in Supporting Information S1) and an average monthly climatology was formed. Annual cycle uncertainties are the standard error of the monthly mean. Significance levels were computed using an effective degrees of freedom determined from an integral time scale (Chapter 3 in Thomson & Emery, 2014).

3. Results and Discussion

3.1. Mean Transport and Trends

Time-mean WBC transport between 0 m and 1975 m over 2004–2019 was −45.0 ± 5.2 Sv (1 Sv ≡ 1×10^6 m^3 s^{-1}) for the Agulhas, −20.9 ± 1.8 Sv for the EAC, and 69.8 ± 8.2 Sv for the Kuroshio (Figures 3a–3c). Our EAC estimate is comparable to nearby shorter period observations in the upper 2000 m of −19.5 ± 2.0 Sv at PX30 over 2004–2015 (Zilberman et al., 2018), −22.1 ± 7.5 Sv near 27°S over 2012–2013 (Sloyan et al., 2016),

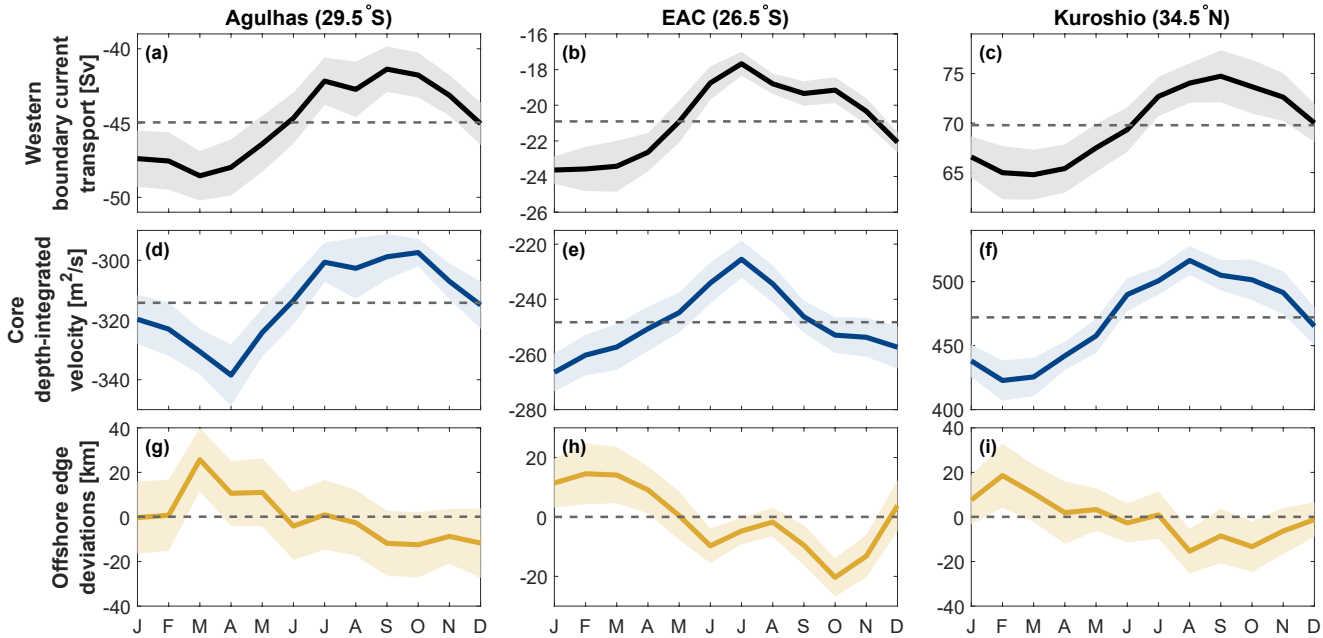

Figure 3. Annual cycles in the Agulhas Current (left), East Australian Current (EAC, middle), and Kuroshio (right) for: (a–c) western boundary current transport (positive values northward); (d–f) core depth-integrated velocity (positive values northward); (g–i) offshore edge deviations (positive values eastward). Shading is ±1 standard error. Dashed line is the 2004–2019 mean.

and −23.67 Sv at 30°S over 1991–1993 (Mata et al., 2000). Our Agulhas cross-transect transport estimate is smaller than the upper 2400 m transport estimate of −76.2 Sv made using direct current measurements near 31°S over a 9 month period in 1995 (Bryden et al., 2005). IX21 is located over a wider section of the continental shelf (Figure 1b) where, during 2004–2019, both Argo trajectory velocities and satellite altimetry surface geostrophic velocities were weaker than the stronger and more coherent poleward velocities associated with the Agulhas Current at the location of the Bryden et al. (2005) mooring array (not shown). In the Kuroshio south of Japan, around 32°N 133°E, a comparable full-depth transport of 65 ± 4 Sv was found over 1993–1995 (Book et al., 2002).

Trends in the raw monthly transport time series over 2004–2019 were only significant (at the 95% confidence interval) in the Kuroshio, which showed a weakening poleward transport (−1.20 ± 0.36 Sv yr^{-1}; Figure S4 in Supporting Information S1) with contributions from both a weakening core depth-integrated velocity (−4.66 ± 2.64 m^2 s^{-1} yr^{-1}) and a narrowing of the offshore edge (−3.27 ± 1.97 km yr^{-1}). Wang et al. (2016) and Liu et al. (2021) also observed a weakening Kuroshio (upstream of Japan) over earlier 1993–2013 and 1998–2013 periods, respectively. This decreasing Kuroshio transport over recent decades has been hypothesized to be caused by a weakening of the negative North Pacific wind stress curl (Liu et al., 2021; Wang et al., 2016) which propagates baroclinic signals into the Kuroshio region, causing a shallower offshore pycnocline depth and relaxation of the pycnocline gradient across the Kuroshio (Liu et al., 2021; Sugimoto et al., 2010). Examination of our velocity trends over 2004–2019 (Figure S5 in Supporting Information S1) suggests that the offshore region of the poleward-flowing Kuroshio has experienced the largest decrease in velocity, consistent with this proposed mechanism. However, as these winds are known to demonstrate multi-decadal variability (Sugimoto et al., 2010; Trenberth et al., 2014) it is uncertain whether the recent decreasing transport trend will continue over future decades. EAC transport showed no significant trend (0.03 ± 0.19 Sv yr^{-1}; positive trend indicates weakening) which could be due to competing influences from a strengthening core depth-integrated velocity (−4.14 ± 1.24 m^2 s^{-1} yr^{-1}) and narrowing of the offshore edge (−2.78 ± 1.54 km yr^{-1}). No other observational EAC transport trends have been published in the literature. However, modeling studies have examined past and future trends and suggest increased transport in the southern EAC and EAC extension (i.e., downstream of PX30) that is driven by strengthening of the positive South Pacific wind stress curl south of where the EAC separates from the coast, and a largely unchanged wind stress curl to the north (Cetina-Heredia et al., 2014; Oliver & Holbrook, 2014). Agulhas transport also showed no significant trend (−0.21 ± 0.37 Sv yr^{-1}; negative trend

indicates strengthening). Beal and Elipot (2016) found a non-significant transport trend downstream of IX21 over 1993–2015, concluding that the Agulhas was instead broadening due to increased eddy activity. We also found a significant broadening trend in the Agulhas offshore edge (3.38 ± 3.19 km yr^{-1}) at IX21, suggesting that this broadening may be happening over the length of the Agulhas Current.

3.2. Annual Cycles

All three WBCs demonstrate a significant transport annual cycle (Figures 3a–3c), accounting for 14%, 25%, and 23% of the variance in the Agulhas, EAC, and Kuroshio respectively. In the southern hemisphere, the Agulhas and EAC are stronger in the austral summer and weaker in the austral winter. Agulhas transport peaks in March (−48.6 ± 1.7 Sv) and is minimum in September (−41.4 ± 1.5 Sv). EAC transport peaks in January (−23.6 ± 0.8 Sv) and is minimum in July (−17.7 ± 0.7 Sv). Other studies have shown comparable timing of the transport annual cycle in both the Agulhas (e.g., Beal & Elipot, 2016; Beal et al., 2015) and EAC (e.g., Kerry & Roughan, 2020; Ridgway & Godfrey, 1997; Zilberman et al., 2018). The smaller amplitude at IX21 than observed further downstream (Beal & Elipot, 2016; Beal et al., 2015) suggests that the amplitude of the Agulhas transport annual cycle increases poleward. In the northern hemisphere, the Kuroshio is stronger in the boreal summer, peaking in September (74.7 ± 2.6 Sv), and weaker in the boreal winter, with a minimum in March (64.8 ± 2.5 Sv). Stronger transport in summer has been observed in the upstream Kuroshio (e.g., Gilson & Roemmich, 2002; Lee et al., 2001; Wei et al., 2015; Zhu et al., 2017), though often with minimum transport in autumn (Lee et al., 2001; Wei et al., 2015; Zhu et al., 2017). Observations of the Kuroshio annual cycle near PX40 have not been published before and we find a much larger amplitude than observed further upstream in the Kuroshio. The different timing of the annual cycle minimum compared to further upstream may be linked to PX40's location east of Izu Ridge (Figure 1d) which blocks barotropic Rossby waves propagating westward from the ocean interior (Lee et al., 2001).

All three WBCs also demonstrate a significant annual cycle in core depth-integrated velocity (Figures 3d–3f), accounting for 15%, 26%, and 33% of the variance in the Agulhas, EAC, and Kuroshio respectively. The timing of these annual cycles are consistent with those for WBC transport, with poleward core depth-integrated velocity at a maximum (minimum) in April (October) in the Agulhas, January (July) in the EAC, and August (February) in the Kuroshio. In contrast, annual cycles are not clear in the offshore edge deviations (Figures 3g–3i). The offshore edge of the Agulhas and Kuroshio hint at an annual cycle but remain close to the mean for almost all months and the annual cycles are not significant, with each explaining only 4% of the variance. The EAC offshore edge demonstrates a significant quasi semiannual cycle, with an offshore maximum in February and onshore maximum in October, that explains 13% of the variance.

Similarities between the WBC transport and core depth-integrated velocity annual cycles, and the lack of any clear annual cycle in offshore edge deviations, suggest that, for all three WBCs, seasonality in WBC transport is driven more by corresponding changes in the speed of the WBC core rather than the width of the WBC. In other words, when the core of the WBC is flowing faster in the summer, the volume transport of the WBC is larger. The converse is true in winter. Whether the similar transport annual cycles are driven by similar forcing mechanisms remains unclear. In the Agulhas, the transport annual cycle is driven by baroclinic adjustment to near-field winds, with the wind-driven barotropic component small (Hutchinson et al., 2018). In the Kuroshio, the annual cycle of velocity above 500 m is dominated by local wind stress, with wind stress curl west of the Izu Ridge (Figure 1d) controlling the barotropic response (Lee et al., 2001; Zhang et al., 2021). The relationship between the EAC annual cycle and wind forcing remains poorly understood (Kerry & Roughan, 2020), although given the similarities in the annual cycles between the three WBCs we may expect local wind stress to be important.

3.3. Temporal Variability in the Location of the WBC

Large offshore displacements in the core of the Agulhas Current occurred irregularly at IX21 (Figure 2a). Following previous studies (e.g., Elipot & Beal, 2015; Krug & Tournadre, 2012; Leber & Beal, 2014; Rouault & Penven, 2011), we defined Natal Pulses (NPs) as when the core longitude meandered offshore by more than 1 standard deviation from the mean (Figure 4a). The SLA composite for months in which NPs were identified (Figure 4e) shows an anomalous cyclonic circulation near the coast and an anomalous anticyclonic circulation offshore. Twenty-one NPs were identified over the 16 year record, varying between 0 and 3 events per year

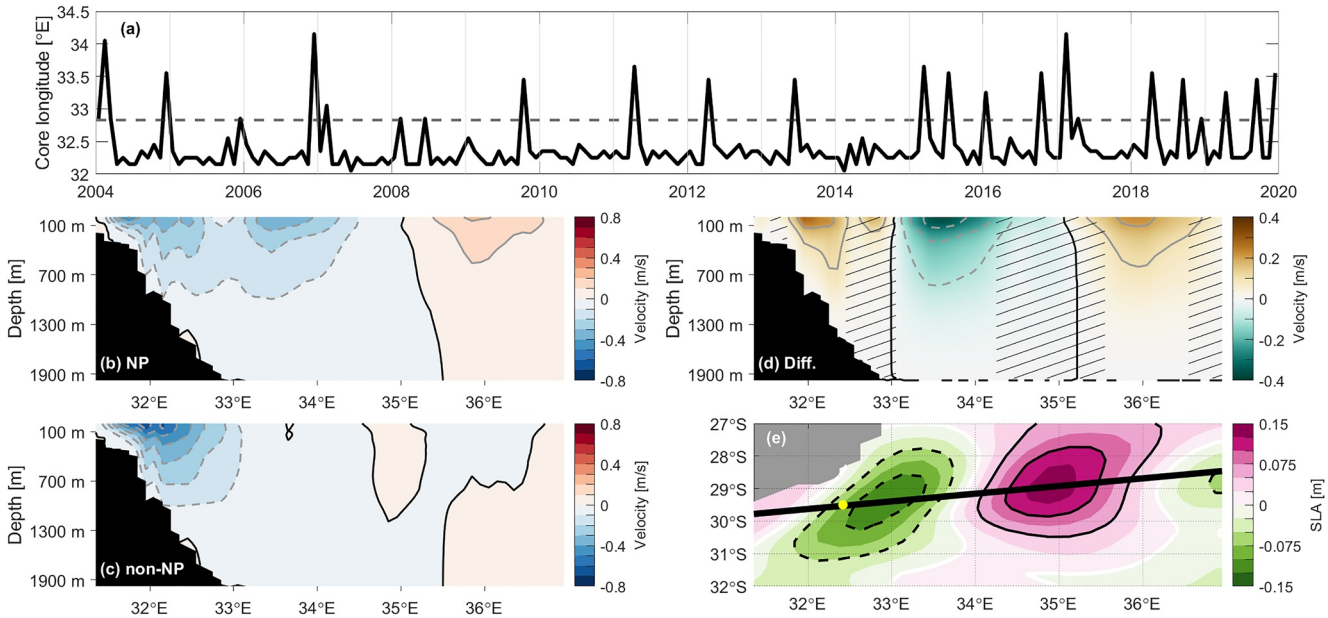

Figure 4. (a) Monthly time series of Agulhas Current core longitude. Dashed line indicates +1 standard deviation from the mean. (b) Absolute cross-transect geostrophic velocity composite for Natal Pulse (NP) events. Negative velocities are poleward. (c) As in (b) but for non-NP periods. (d) Difference between the two composites (NP minus non-NP). Hatching indicates where differences are not significant at the 95% confidence level. For (b–d) the black contour denotes 0 m s^{-1} and the solid and dashed gray contours are at intervals of +0.1 and −0.1 m s^{-1}. (e) Composite of monthly sea level anomaly (SLA) for NP months. The black line is the IX21 nominal transect and the yellow marker the mean location of the Agulhas Current core. The white SLA contour denotes 0 m and the solid and dashed black SLA contours are at intervals of +0.05 and −0.05 m.

and with an average of 1.3 per year. This rate is slightly lower than the average of 1.5–2 per year further downstream (Elipot & Beal, 2015; Krug & Tournadre, 2012; Rouault & Penven, 2011), but slightly higher than the approximately 1 per year near IX21 (Rouault & Penven, 2011). Our velocity cross-section composites at IX21 (Figures 4b–4d) show poleward flow in the Agulhas is stronger and closer to the coast under normal conditions (maximum poleward velocity of 0.66 m s^{-1}; Figure 4c) compared to when a NP is present (maximum poleward velocity of 0.51 m s^{-1}; Figure 4b). In the NP composite (Figure 4b) there are two separate cores with poleward velocities greater than 0.1 m s^{-1} down to 950 m depth. This two-core structure is likely an artifact of the monthly sampling resolution, as any given month may experience both NP and non-NP conditions. For example, Elipot and Beal (2015) found NPs took between 23 and 44 days to cross their mooring array. The surface-intensified recirculation centered around 36°E is likely tied to the anticyclonic surface anomaly (Figure 4e). Under normal conditions (Figure 4c), poleward velocities greater than 0.1 m s^{-1} reached 1000 m depth.

In the North Pacific, the Kuroshio-Kuroshio Extension (KE) system is known to vary between dynamically stable and unstable states on decadal time scales due to a negative feedback with the North Pacific wind stress curl (Qiu & Chen, 2005, 2010; Qiu et al., 2014, 2020). Qiu et al. (2014) introduced the Kuroshio Extension Index (KEI; Figure S6 in Supporting Information S1), which uses satellite altimetry to provide a single measure of this low frequency variability in the KE. Satellite observations suggest that the Kuroshio typically passes through a gap in the Izu Ridge (Figure 1d) closer to the coast during a stable dynamic state (positive KEI) and over the ridge further offshore during an unstable dynamic state (negative KEI) (Qiu & Chen, 2005). Our composites of the velocity cross-section at PX40, downstream of the Izu Ridge, show that the structure of the poleward-flowing Kuroshio is similar during both positive and negative KEI states (Figure 5). These similarities are indicative of the convergence of the different Kuroshio pathways downstream of the Izu Ridge (Kawabe, 1995). Likewise, both WBC transport and maximum poleward velocities were statistically similar (at the 95% confidence level) between the two composites (70.5 Sv and 0.89 m s^{-1} for the positive KEI compared to 72.9 Sv and 0.83 m s^{-1} for the negative KEI). The largest differences occurred further offshore, with significantly stronger equatorward velocities between 144.05°E and 145.05°E and poleward velocities between 145.85°E and 147.45°E in the negative KEI composite (Figures 5b and 5c). In an unstable dynamic state the KE is located further south, therefore

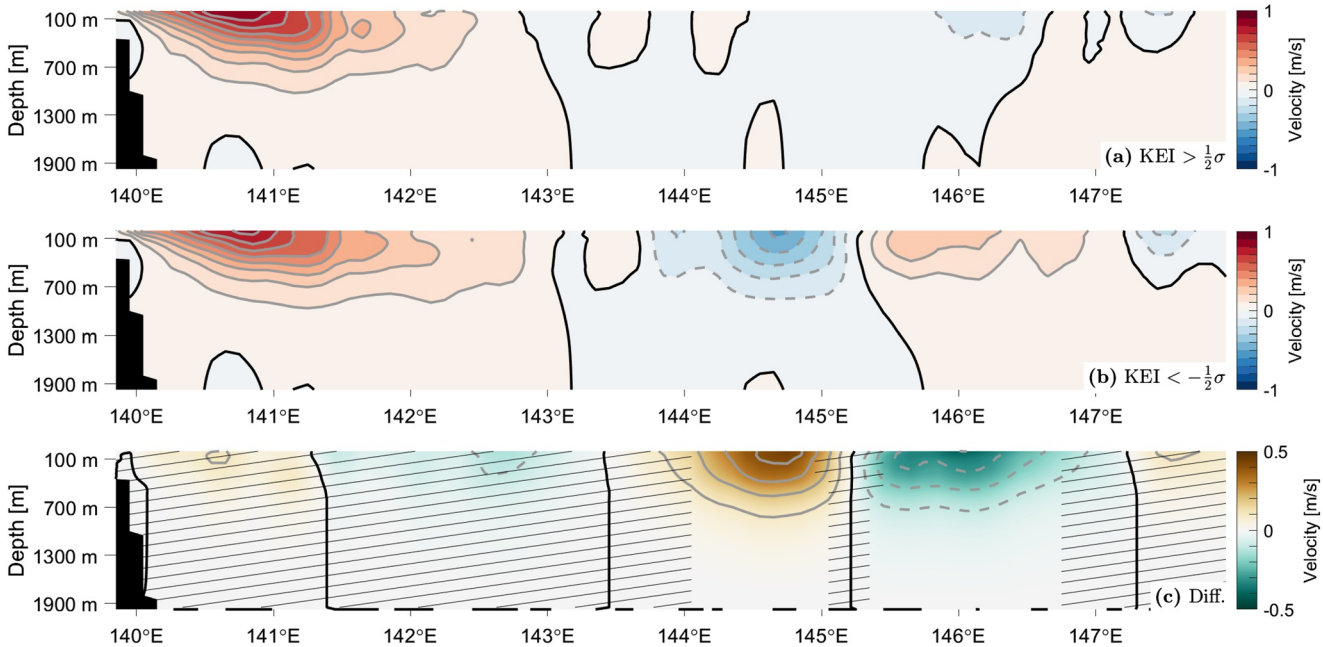

Figure 5. (a) Absolute cross-transect geostrophic velocity composite for periods when the Kuroshio Extension Index (KEI) is positive $\left(>\frac{1}{2}\sigma\right)$. Positive velocities are poleward. (b) As in (a) but for negative KEI $\left(<-\frac{1}{2}\sigma\right)$. (c) Difference between the two composites (positive minus negative). Hatching indicates where differences are not significant at the 95% confidence level. For (a–c) the black contour denotes 0 m s^{-1} and the solid and dashed gray contours are at intervals of +0.1 and −0.1 m s^{-1}.

closer to PX40, and exhibits greater meandering (Qiu & Chen, 2010; Qiu et al., 2014). As such, meanders in the KE more readily intersect PX40. The opposite occurs during a stable dynamic state.

In contrast to both the Agulhas and Kuroshio, the location of the EAC core (Figure 2b) was relatively stable at the location of PX30 which coincides with where the EAC jet is most coherent (Kerry & Roughan, 2020).

4. Conclusions

We examined seasonal-to-decadal variability in the subsurface signature of the Agulhas Current, EAC, and Kuroshio using 16 year time series produced from sustained ocean observations. Few other observational studies of these WBCs span time periods of a similar length or longer (e.g., Beal & Elipot, 2016; Liu et al., 2021; Oka et al., 2018; Ridgway et al., 2008; Wei et al., 2015). Uniquely, our application of a consistent methodology permits direct comparison of velocity and transport variability in the upper 1975 m of WBCs. Given the sparse distribution of Argo data, we are unable to resolve any trends or variability in the barotropic signal using Argo trajectories and therefore a constant reference level was used. However, the envisioned increase in Argo sampling density in WBC regions (Roemmich et al., 2019) may allow for a time-varying reference level that addresses these limitations in the future.

Decreased Kuroshio transport and no significant change in EAC or Agulhas transport were observed over 2004–2019. As noted above, there are relatively few long time series that can provide comparisons with these observed trends. Our time series provide a baseline for studying future changes and therefore contribute toward addressing this long-term observations knowledge gap. Transport annual cycles were remarkably similar in all three WBCs, with poleward transport stronger in the summer and weaker in the winter. Our results suggest that this summertime transport maximum is driven by an increase in current speed rather than current width. Importantly, the length of our time series provide enhanced confidence in the robustness of these observed annual cycles.

Incorporating subsurface observations allows us to expand upon sea surface satellite observations of variability in the path of WBCs (e.g., Krug & Tournadre, 2012; Qiu & Chen, 2005, 2010; Qiu et al., 2014; Rouault & Penven, 2011). Observing the vertical structure of velocity down to 1975 m depth provides context for these

satellite altimetry studies as the subsurface flow is not required to follow the surface expression. Variability in the Agulhas core longitude was dominated by NPs that occurred at an average rate of 1.3 per year. The subsurface velocity structure showed that, during NPs, the Agulhas was slower near the coast and faster offshore, with differences of 0.1 m s^{-1} as deep as 800 m when compared with normal conditions. At PX40, the poleward-flowing Kuroshio was found to be similar during both positive and negative KEI states, however differences in the meandering of the KE were evident further offshore with 0.1 m s^{-1} differences also extending to 800 m depth. Variability in WBC location may influence ocean temperature advection and air-sea interactions, with important implications for both ocean temperature and regional weather patterns (e.g., Oliver et al., 2021; Sugimoto et al., 2021).

Our work demonstrates the ability of the Zilberman et al. (2018) method to provide a consistent procedure for examining and comparing subsurface variability in WBCs. The time series we produced are longer than most other observations in these WBCs and therefore provide enhanced confidence in the robustness of observed variability. Because the high spatial resolution observations needed to observe WBCs are provided by HR-XBT transects, which are present in all ocean basins (Goni et al., 2019), this method can be applied to illuminate variability in other boundary currents. Furthermore, incorporating autonomous underwater gliders - which provide sustained and high spatial resolution observations from the surface down to 1000 m depth (Rudnick, 2016; Testor et al., 2019) - in place of HR-XBT transects could allow the method to be applied in other regions. These long-term observations of WBCs will be important for studying the impact of WBC variability on, for example, marine heatwaves and local sea-level variability.

Data Availability Statement

The HR-XBT data is made available by the Scripps Institution of Oceanography HR-XBT program (IX21 - http://www-hrx.ucsd.edu/ix15.html; PX30 - http://www-hrx.ucsd.edu/px31.html; PX40 - http://www-hrx.ucsd.edu/px40.html). The Argo data is collected and made available by the International Argo Program and the national programs that contribute to it (https://doi.org/10.17882/42182). The Argo temperature and salinity climatologies are available from http://sio-argo.ucsd.edu/RG_Climatology.html. The satellite altimetry products are available from the EU Copernicus Marine Service (https://doi.org/10.48670/moi-00148). Bathymetry data is available through the NOAA National Centers for Environmental Information (https://doi.org/10.7289/V5J1012Q). The first surface mode deformation radius data set is available from https://figshare.com/articles/dataset/Rossby_Deformation_Radius/14336759. Data from the Kuroshio Extension System Study can be accessed through the program websites (http://www.po.gso.uri.edu/dynamics/kess/CPIES_data.html and https://uskess.whoi.edu/overview/dataproducts/). Scripts for building the velocity estimates and conducting the analysis are publicly available at MC's GitHub (https://github.com/mlchandler/wbc_sustained_obs). The velocity time series produced from this research are permanently available through Zenodo (https://doi.org/10.5281/zenodo.5851311).

Acknowledgments
The authors thank Lisa Lehmann and Megan Scanderbeg for their assistance with some of the data processing, Bo Qiu for providing the KEI, Kathleen Donohue for providing data from the Kuroshio Extension System Study, and Bernadette Sloyan for providing the EAC mooring array data. The authors also thank two anonymous reviewers for their comments which helped to improve the manuscript. This study was supported by NOAA's Global Ocean Monitoring and Observing Program. NZ and JS were supported by the NOAA Global Ocean Monitoring and Observing Program through Award NA20OAR4320278. NZ was supported by the National Oceanographic Partnership Program (NOAA grant NA18OAR0110434). MC received financial support from Fulbright New Zealand.

References

Archer, M. R., Shay, L. K., & Johns, W. E. (2017). The surface velocity structure of the Florida Current in a jet coordinate frame. *Journal of Geophysical Research: Oceans*, *122*, 9189–9208. https://doi.org/10.1002/2017JC013286

Beal, L. M., & Elipot, S. (2016). Broadening not strengthening of the Agulhas Current since the early 1990s. *Nature*, *540*(7634), 570–573. https://doi.org/10.1038/nature19853

Beal, L. M., Elipot, S., Houk, A., & Leber, G. M. (2015). Capturing the transport variability of a western boundary jet: Results from the Agulhas Current Time-series experiment (ACT). *Journal of Physical Oceanography*, *45*(5), 1302–1324. https://doi.org/10.1175/JPO-D-14-0119.1

Book, J. W., Wimbush, M., Imawaki, S., Ichikawa, H., Uchida, H., & Kinoshita, H. (2002). Kuroshio temporal and spatial variations south of Japan determined from inverted echo sounder measurements. *Journal of Geophysical Research*, *107*, 3121. https://doi.org/10.1029/2001JC000795

Bryden, H. L., Beal, L. M., & Duncan, L. M. (2005). Structure and transport of the Agulhas Current and its temporal variability. *Journal of Oceanography*, *61*(3), 479–492. https://doi.org/10.1007/s10872-005-0057-8

Cetina-Heredia, P., Roughan, M., vanSebille, E., & Coleman, M. A. (2014). Long-term trends in the East Australian Current separation latitude and eddy driven transport. *Journal of Geophysical Research: Oceans*, *119*, 4351–4366. https://doi.org/10.1002/2014JC010071

Cronin, M. F., Bond, N., Booth, J., Ichikawa, H., Joyce, T. M., Kelly, K., et al. (2010). Monitoring ocean - atmosphere interactions in western boundary current extensions. In *Proceedings of OceanObs'09: Sustained ocean observations and information for society* (Vol. 2, pp. 199–209). European Space Agency. https://doi.org/10.5270/OceanObs09.cwp.20

Diabaté, S. T., Swingedouw, D., Hirschi, J. J.-M., Duchez, A., Leadbitter, P. J., Haigh, I. D., & McCarthy, G. D. (2021). Western boundary circulation and coastal sea-level variability in Northern Hemisphere oceans. *Ocean Science*, *17*(5), 1449–1471. https://doi.org/10.5194/os-17-1449-2021

Donohue, K. A., Watts, D. R., Tracey, K., Wimbush, M., Park, J.-H., Bond, N., et al. (2008). Program studies the Kuroshio extension. *Eos, Transactions American Geophysical Union*, *89*(17), 161–162. https://doi.org/10.1029/2008EO170002

Donohue, K. A., Watts, D. R., Tracey, K. L., Greene, A. D., & Kennelly, M. (2010). Mapping circulation in the Kuroshio extension with an array of current and pressure recording inverted echo sounders. *Journal of Atmospheric and Oceanic Technology*, *27*(3), 507–527. https://doi.org/10.1175/2009JTECHO686.1

Elipot, S., & Beal, L. M. (2015). Characteristics, energetics, and origins of Agulhas Current meanders and their limited influence on ring shedding. *Journal of Physical Oceanography*, *45*(9), 2294–2314. https://doi.org/10.1175/JPO-D-14-0254.1

Ezer, T., Atkinson, L. P., Corlett, W. B., & Blanco, J. L. (2013). Gulf Stream's induced sea level rise and variability along the U.S. mid-Atlantic coast. *Journal of Geophysical Research: Oceans*, *118*, 685–697. https://doi.org/10.1002/jgrc.20091

Gill, A. E. (1982). *Atmosphere-ocean dynamics*. Academic Press.

Gilson, J., & Roemmich, D. (2002). Mean and temporal variability in Kuroshio geostrophic transport South of Taiwan (1993–2001). *Journal of Oceanography*, *58*(1), 183–195. https://doi.org/10.1023/A:1015841120927

Goes, M., Goni, G., Dong, S., Boyer, T., & Baringer, M. (2020). The complementary value of XBT and Argo observations to monitor ocean boundary currents and meridional heat and volume transports: A case study in the Atlantic Ocean. *Journal of Atmospheric and Oceanic Technology*, *37*(12), 1–42. https://doi.org/10.1175/JTECH-D-20-0027.1

Goni, G. J., Sprintall, J., Bringas, F., Cheng, L., Cirano, M., Dong, S., et al. (2019). More than 50 Years of successful continuous temperature section measurements by the global expendable bathythermograph network, its integrability, societal benefits, and future. *Frontiers in Marine Science*, *6*. https://doi.org/10.3389/fmars.2019.00452

Holbrook, N. J., Goodwin, I. D., McGregor, S., Molina, E., & Power, S. B. (2011). ENSO to multi-decadal time scale changes in East Australian Current transports and Fort Denison sea level: Oceanic Rossby waves as the connecting mechanism. *Deep Sea Research Part II: Topical Studies in Oceanography*, *58*(5), 547–558. https://doi.org/10.1016/j.dsr2.2010.06.007

Hu, D., Wu, L., Cai, W., Gupta, A. S., Ganachaud, A., Qiu, B., et al. (2015). Pacific western boundary currents and their roles in climate. *Nature*, *522*(7556), 299–308. https://doi.org/10.1038/nature14504

Hutchinson, K., Beal, L. M., Penven, P., Ansorge, I., & Hermes, J. (2018). Seasonal phasing of Agulhas Current transport tied to a baroclinic adjustment of near-field winds. *Journal of Geophysical Research: Oceans*, *123*, 7067–7083. https://doi.org/10.1029/2018JC014319

Kawabe, M. (1995). Variations of current path, velocity, and volume transport of the Kuroshio in relation with the large meander. *Journal of Physical Oceanography*, *25*(12), 3103–3117. https://doi.org/10.1175/1520-0485(1995)025<3103:vocpva>2.0.co;2

Kerry, C., & Roughan, M. (2020). Downstream evolution of the East Australian Current system: Mean flow, seasonal, and intra-annual variability. *Journal of Geophysical Research: Oceans*, *125*, e2019JC015227. https://doi.org/10.1029/2019JC015227

Krug, M., & Tournadre, J. (2012). Satellite observations of an annual cycle in the Agulhas Current. *Geophysical Research Letters*, *39*(15). https://doi.org/10.1029/2012GL052335

LaCasce, J. H., & Groeskamp, S. (2020). Baroclinic modes over rough bathymetry and the surface deformation radius. *Journal of Physical Oceanography*, *50*(10), 2835–2847. https://doi.org/10.1175/JPO-D-20-0055.1

Leber, G. M., & Beal, L. M. (2014). Evidence that Agulhas Current transport is maintained during a meander. *Journal of Geophysical Research: Oceans*, *119*, 3806–3817. https://doi.org/10.1002/2014JC009802

Lee, T. N., Johns, W. E., Liu, C.-T., Zhang, D., Zantopp, R., & Yang, Y. (2001). Mean transport and seasonal cycle of the Kuroshio east of Taiwan with comparison to the Florida Current. *Journal of Geophysical Research*, *106*(C10), 22143–22158. https://doi.org/10.1029/2000JC000535

Liu, Z.-J., Zhu, X.-H., Nakamura, H., Nishina, A., Wang, M., & Zheng, H. (2021). Comprehensive observational features for the Kuroshio transport decreasing trend during a recent global warming hiatus. *Geophysical Research Letters*, *48*(18), e2021GL094169. https://doi.org/10.1029/2021GL094169

Mata, M. M., Tomczak, M., Wijffels, S., & Church, J. A. (2000). East Australian Current volume transports at 30°S: Estimates from the World Ocean Circulation Experiment hydrographic sections PR11/P6 and the PCM3 current meter array. *Journal of Geophysical Research*, *105*(C12), 28509–28526. https://doi.org/10.1029/1999JC000121

Minobe, S., Kuwano-Yoshida, A., Komori, N., Xie, S.-P., & Small, R. J. (2008). Influence of the Gulf Stream on the troposphere. *Nature*, *452*(7184), 206–209. https://doi.org/10.1038/nature06690

Nakamura, H., Sampe, T., Goto, A., Ohfuchi, W., & Xie, S.-P. (2008). On the importance of midlatitude oceanic frontal zones for the mean state and dominant variability in the tropospheric circulation. *Geophysical Research Letters*, *35*(15), L15709. https://doi.org/10.1029/2008GL034010

Nhantumbo, B. J., Nilsen, J. E. Ø., Backeberg, B. C., & Reason, C. J. C. (2020). The relationship between coastal sea level variability in South Africa and the Agulhas Current. *Journal of Marine Systems*, *211*, 103422. https://doi.org/10.1016/j.jmarsys.2020.103422

Njouodo, A. S. N., Koseki, S., Keenlyside, N., & Rouault, M. (2018). Atmospheric signature of the Agulhas Current. *Geophysical Research Letters*, *45*(10), 5185–5193. https://doi.org/10.1029/2018GL077042

Oka, E., Ishii, M., Nakano, T., Suga, T., Kouketsu, S., Miyamoto, M., et al. (2018). Fifty years of the 137°E repeat hydrographic section in the western North Pacific Ocean. *Journal of Oceanography*, *74*(2), 115–145. https://doi.org/10.1007/s10872-017-0461-x

Oliver, E. C. J., Benthuysen, J. A., Bindoff, N. L., Hobday, A. J., Holbrook, N. J., Mundy, C. N., & Perkins-Kirkpatrick, S. E. (2017). The unprecedented 2015/16 Tasman Sea marine heatwave. *Nature Communications*, *8*(1), 16101. https://doi.org/10.1038/ncomms16101

Oliver, E. C. J., Benthuysen, J. A., Darmaraki, S., Donat, M. G., Hobday, A. J., Holbrook, N. J., et al. (2021). Marine heatwaves. *Annual Review of Marine Science*, *13*(1), 313–342. https://doi.org/10.1146/annurev-marine-032720-095144

Oliver, E. C. J., & Holbrook, N. J. (2014). Extending our understanding of South Pacific gyre "spin-up": Modeling the East Australian Current in a future climate. *Journal of Geophysical Research: Oceans*, *119*, 2788–2805. https://doi.org/10.1002/2013JC009591

Qiu, B., & Chen, S. (2005). Variability of the Kuroshio extension jet, recirculation gyre, and mesoscale eddies on decadal time scales. *Journal of Physical Oceanography*, *35*(11), 2090–2103. https://doi.org/10.1175/JPO2807.1

Qiu, B., & Chen, S. (2010). Eddy-mean flow interaction in the decadally modulating Kuroshio Extension system. *Deep Sea Research Part II: Topical Studies in Oceanography*, *57*(13), 1098–1110. https://doi.org/10.1016/j.dsr2.2008.11.036

Qiu, B., Chen, S., Schneider, N., Oka, E., & Sugimoto, S. (2020). On the reset of the wind-forced decadal Kuroshio extension variability in late 2017. *Journal of Climate*, *33*(24), 10813–10828. https://doi.org/10.1175/JCLI-D-20-0237.1

Qiu, B., Chen, S., Schneider, N., & Taguchi, B. (2014). A coupled decadal prediction of the dynamic state of the Kuroshio extension system. *Journal of Climate*, *27*(4), 1751–1764. https://doi.org/10.1175/JCLI-D-13-00318.1

Ridgway, K. R., Coleman, R. C., Bailey, R. J., & Sutton, P. (2008). Decadal variability of East Australian Current transport inferred from repeated high-density XBT transects, a CTD survey and satellite altimetry. *Journal of Geophysical Research*, *113*, C08039. https://doi.org/10.1029/2007JC004664

Ridgway, K. R., & Godfrey, J. S. (1997). Seasonal cycle of the East Australian Current. *Journal of Geophysical Research*, *102*(C10), 22921–22936. https://doi.org/10.1029/97JC00227

Riser, S. C., Freeland, H. J., Roemmich, D., Wijffels, S., Troisi, A., Belbéoch, M., et al. (2016). Fifteen years of ocean observations with the global Argo array. *Nature Climate Change*, *6*(2), 145–153. https://doi.org/10.1038/nclimate2872

Roemmich, D. (1983). Optimal estimation of hydrographic station data and derived fields. *Journal of Physical Oceanography*, *13*(8), 1544–1549. https://doi.org/10.1175/1520-0485(1983)013<1544:oeohsd>2.0.co;2

Roemmich, D., Alford, M. H., Claustre, H., Johnson, K., King, B., Moum, J., et al. (2019). On the future of Argo: A global, full-depth, multi-disciplinary array. *Frontiers in Marine Science*, *6*. https://doi.org/10.3389/fmars.2019.00439

Roemmich, D., & Gilson, J. (2009). The 2004–2008 mean and annual cycle of temperature, salinity, and steric height in the global ocean from the Argo Program. *Progress in Oceanography*, *82*(2), 81–100. https://doi.org/10.1016/j.pocean.2009.03.004

Rouault, M. J., & Penven, P. (2011). New perspectives on Natal Pulses from satellite observations. *Journal of Geophysical Research*, *116*, 2010JC006866. https://doi.org/10.1029/2010JC006866

Rudnick, D. L. (2016). Ocean research enabled by underwater gliders. *Annual Review of Marine Science*, *8*(1), 519–541. https://doi.org/10.1146/annurev-marine-122414-033913

Sasaki, Y. N., Minobe, S., & Miura, Y. (2014). Decadal sea-level variability along the coast of Japan in response to ocean circulation changes. *Journal of Geophysical Research: Oceans*, *119*, 266–275. https://doi.org/10.1002/2013JC009327

Scanderbeg, M., Rannou, J.-P., Buck, J., Schmid, C., Gilson, J., & Swift, D. (2019). Argo DAC trajectory cookbook. https://doi.org/10.13155/29824

Send, U., Davis, R., Fischer, J., Imawaki, S., Kessler, W., Meinen, C., et al. (2010). A global boundary current circulation observing network. In *Proceedings of OceanObs'09: Sustained ocean observations and information for society* (Vol. 2). European Space Agency. https://doi.org/10.5270/OceanObs09.cwp.78

Sen Gupta, A., Stellema, A., Pontes, G. M., Taschetto, A. S., Vergés, A., & Rossi, V. (2021). Future changes to the upper ocean Western Boundary Currents across two generations of climate models. *Scientific Reports*, *11*(1), 9538. https://doi.org/10.1038/s41598-021-88934-w

Sloyan, B. M., Ridgway, K. R., & Cowley, R. (2016). The East Australian Current and property transport at 27°S from 2012 to 2013. *Journal of Physical Oceanography*, *46*(3), 993–1008. https://doi.org/10.1175/JPO-D-15-0052.1

Smith, W. H. F., & Sandwell, D. T. (1997). Global sea floor topography from satellite altimetry and ship depth soundings. *Science*, *277*(5334), 1956–1962. https://doi.org/10.1126/science.277.5334.1956

Sugimoto, S., Hanawa, K., Narikiyo, K., Fujimori, M., & Suga, T. (2010). Temporal variations of the net Kuroshio transport and its relation to atmospheric variations. *Journal of Oceanography*, *66*(5), 611–619. https://doi.org/10.1007/s10872-010-0050-8

Sugimoto, S., Qiu, B., & Schneider, N. (2021). Local atmospheric response to the Kuroshio large meander path in summer and its remote influence on the climate of Japan. *Journal of Climate*, *34*(9), 3571–3589. https://doi.org/10.1175/JCLI-D-20-0387.1

Taburet, G., Sanchez-Roman, A., Ballarotta, M., Pujol, M.-I., Legeais, J.-F., Fournier, F., et al. (2019). DUACS DT2018: 25 years of reprocessed sea level altimetry products. *Ocean Science*, *15*(5), 1207–1224. https://doi.org/10.5194/os-15-1207-2019

Testor, P., de Young, B., Rudnick, D. L., Glenn, S., Hayes, D., Lee, C. M., et al. (2019). OceanGliders: A component of the integrated GOOS. *Frontiers in Marine Science*, *6*, 422. https://doi.org/10.3389/fmars.2019.00422

Thomson, R. E., & Emery, W. J. (2014). *Data analysis methods in physical oceanography* (3rd ed.). Elsevier.

Trenberth, K. E., Fasullo, J. T., Branstator, G., & Phillips, A. S. (2014). Seasonal aspects of the recent pause in surface warming. *Nature Climate Change*, *4*(10), 911–916. https://doi.org/10.1038/nclimate2341

Wang, Y.-L., Wu, C.-R., & Chao, S.-Y. (2016). Warming and weakening trends of the Kuroshio during 1993–2013. *Geophysical Research Letters*, *43*(17), 9200–9207. https://doi.org/10.1002/2016GL069432

Wei, Y., Pei, Y., & Zhang, R.-H. (2015). Seasonal variability of the Kuroshio current at the PN section in the East China sea based on in-situ observation from 1987 to 2010. *Acta Oceanologica Sinica*, *34*(5), 12–21. https://doi.org/10.1007/s13131-015-0662-3

Yang, H., Lohmann, G., Wei, W., Dima, M., Ionita, M., & Liu, J. (2016). Intensification and poleward shift of subtropical western boundary currents in a warming climate. *Journal of Geophysical Research: Oceans*, *121*, 4928–4945. https://doi.org/10.1002/2015JC011513

Zhang, Z.-L., Nakamura, H., & Zhu, X.-H. (2021). Seasonal velocity variations over the entire Kuroshio path part I: Data analysis and numerical experiments. *Journal of Oceanography*, *77*(5), 719–744. https://doi.org/10.1007/s10872-021-00604-7

Zhu, X.-H., Nakamura, H., Dong, M., Nishina, A., & Yamashiro, T. (2017). Tidal currents and Kuroshio transport variations in the Tokara Strait estimated from ferryboat ADCP data. *Journal of Geophysical Research: Oceans*, *122*, 2120–2142. https://doi.org/10.1002/2016JC012329

Zilberman, N. V., Roemmich, D. H., Gille, S. T., & Gilson, J. (2018). Estimating the velocity and transport of western boundary current systems: A case study of the East Australian Current near Brisbane. *Journal of Atmospheric and Oceanic Technology*, *35*(6), 1313–1329. https://doi.org/10.1175/JTECH-D-17-0153.1